



Supplement of

Evaluation of interactive and prescribed agricultural ammonia emissions for simulating atmospheric composition in CAM-chem

Julius Vira et al.

Correspondence to: Julius Vira (julius.vira@gmail.com)

The copyright of individual parts of the supplement might differ from the article licence.

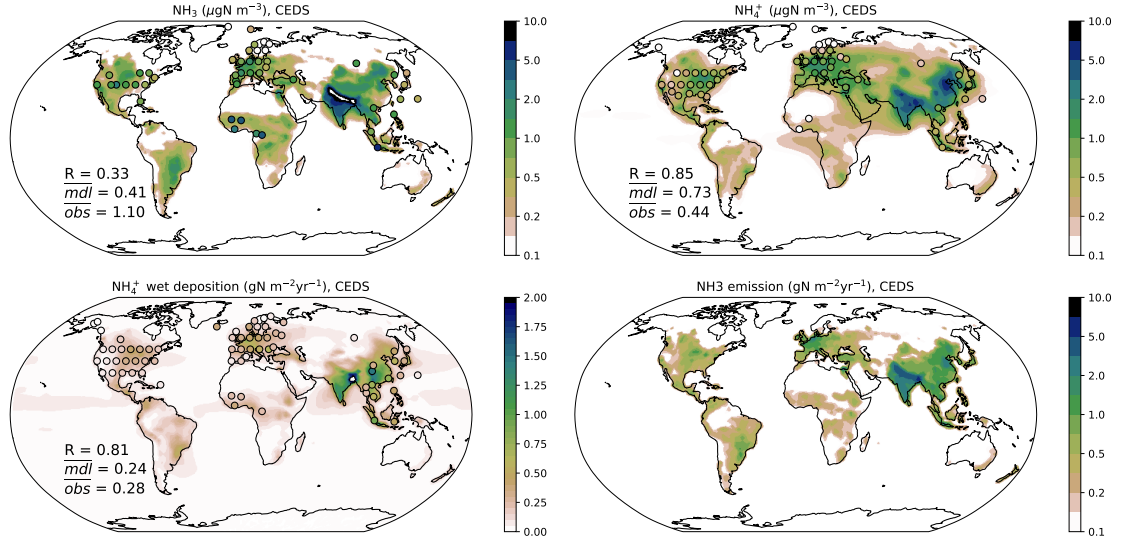


Figure S1: Simulated global distribution for 2010–2015 in the CEDS run: ammonia and ammonium ($\mu\text{gN m}^{-3}$, panels a and b), wet deposition of ammonium and emission of ammonia ($\mu\text{gN m}^{-2} \text{yr}^{-1}$ panels c and d). Markers indicate observed values. The density of observations has been reduced by averaging into a 8-degree grid where necessary. Correlation coefficient (R), average of observations, and model average at observed sites are shown for panels a-c. The statistical parameters are evaluated after the spatial averaging to the 8-degree grid.

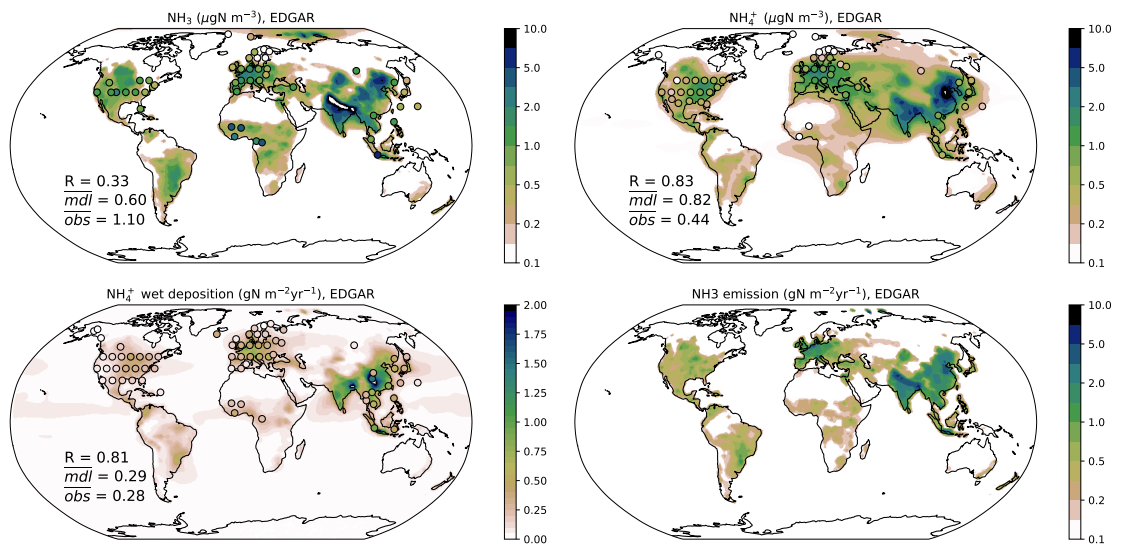


Figure S2: Same as Fig. S1 but for the EDGAR run.

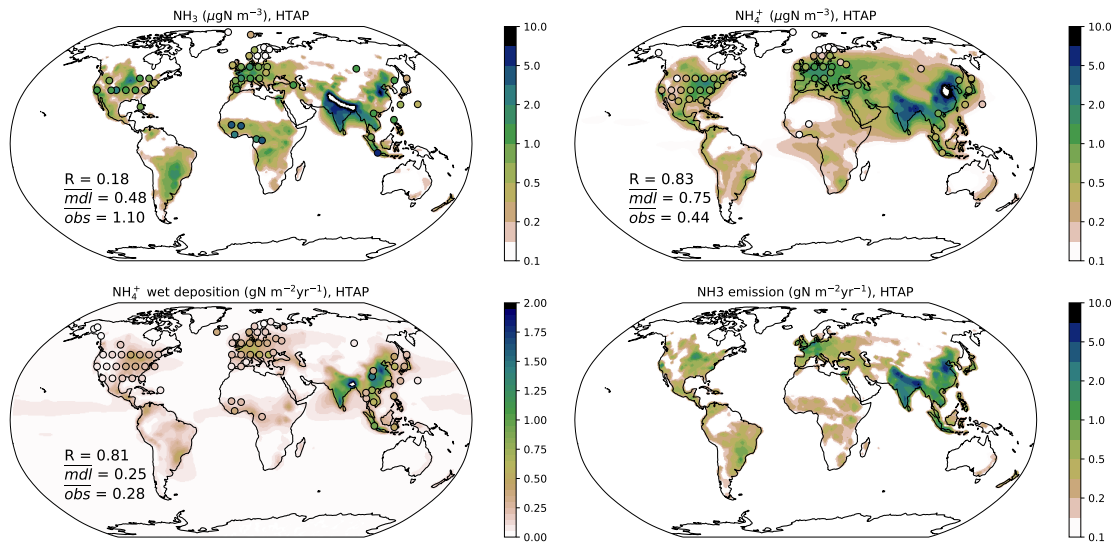


Figure S3: Same as Fig. S1 but for the HTAP run.

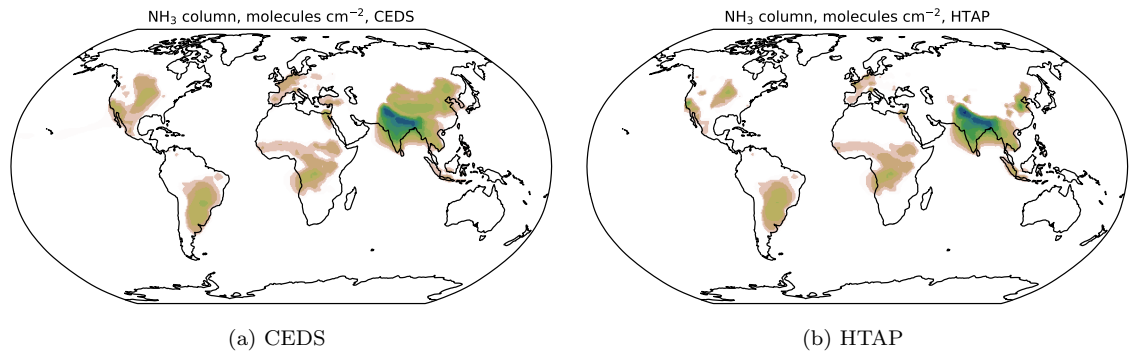


Figure S4: Average column density of NH₃ (molecules cm⁻²) in the (a) CEDS and (b) HTAP simulations for 2010–2015. The results for FAN and EDGAR are shown in Fig. 2.

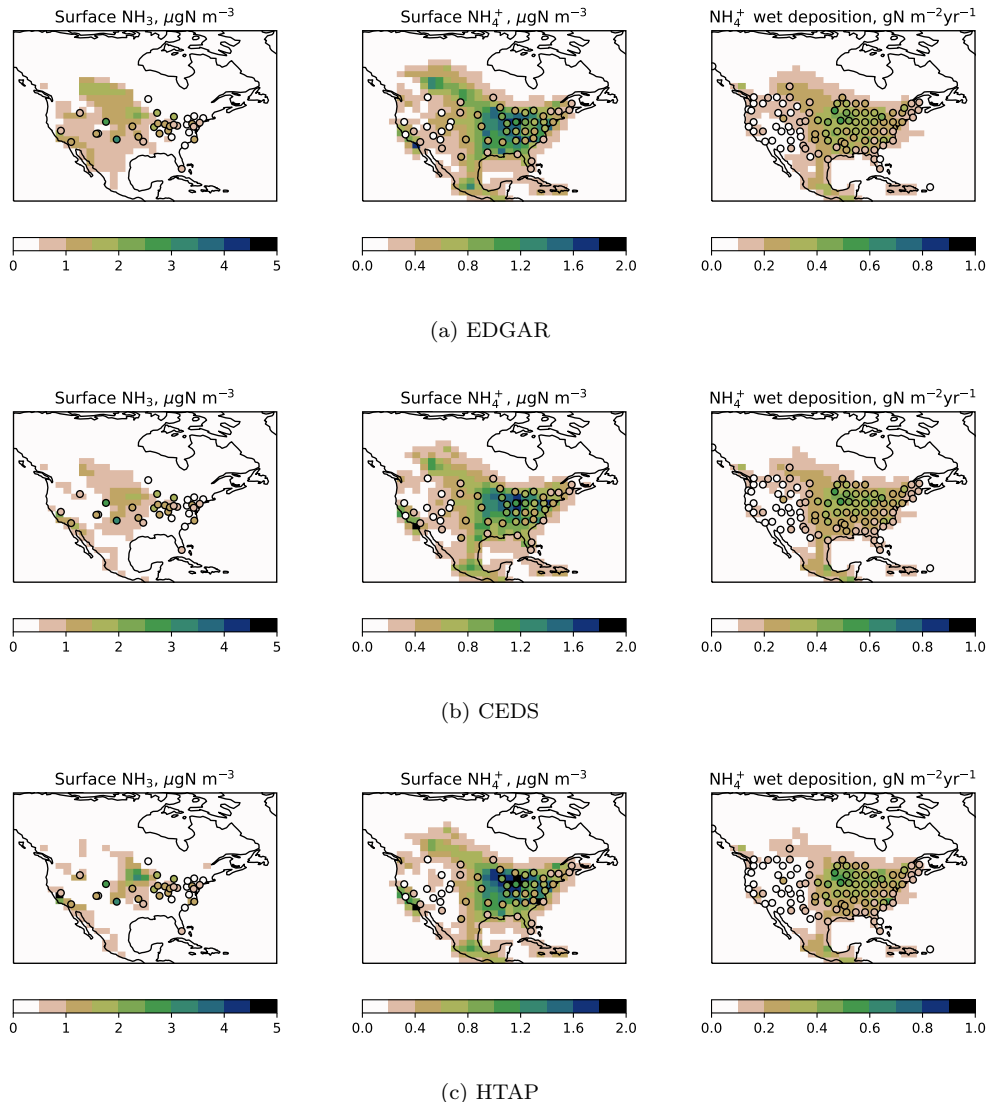


Figure S5: Ammonia (left), ammonium (middle), and wet deposition of ammonium (right) in the EDGAR (a), CEDS (b) and HTAP (c) simulation for North America. Observed values are shown by markers.

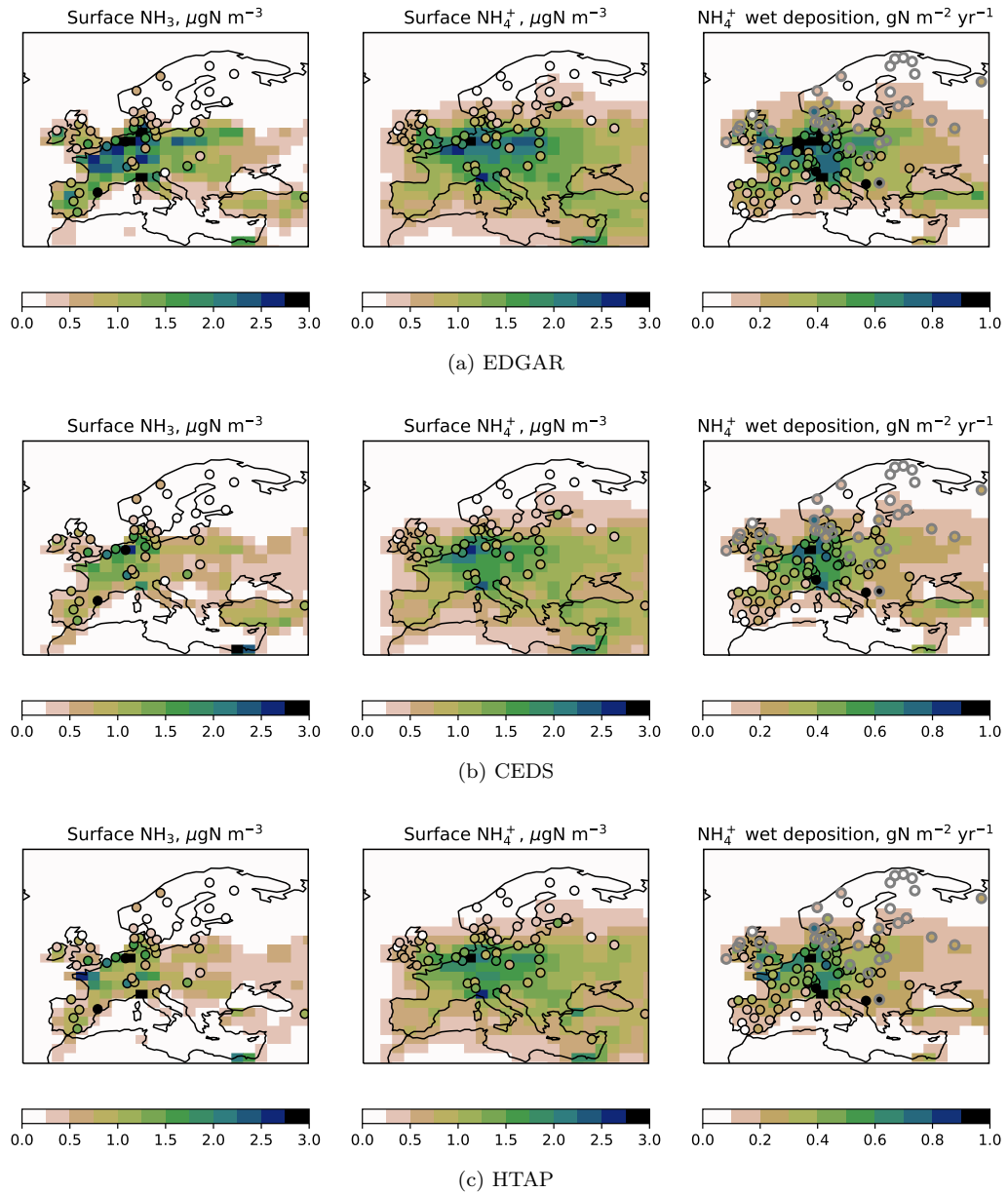


Figure S6: Same as Fig. S5, but for Europe. Grey markers denote wet deposition observations from bulk samplers which are not used for calculating statistical parameters.

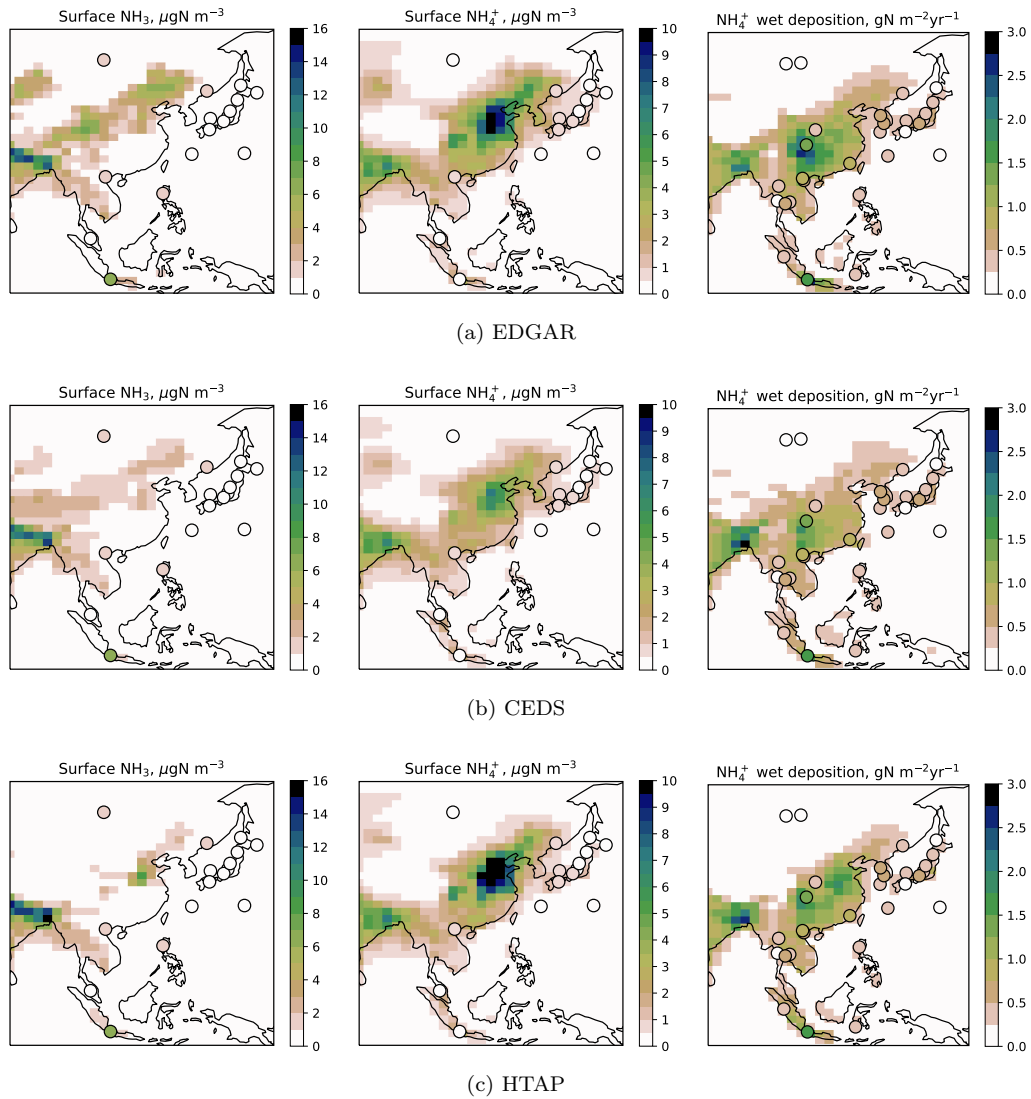


Figure S7: Same as Fig. S5, but for East Asia.

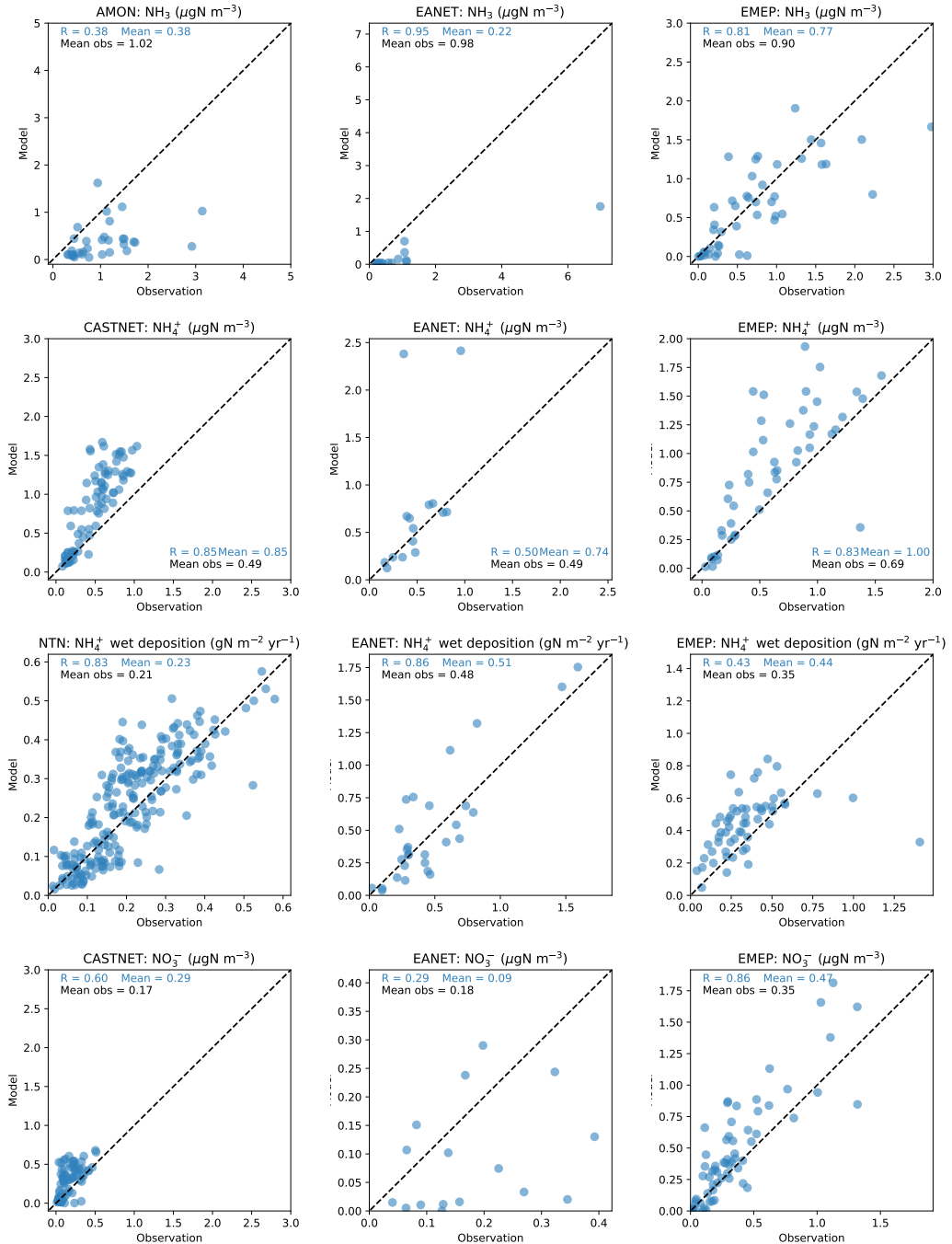


Figure S8: Scatter plots of modeled (FAN) and observed airborne ammonia (top), ammonium (middle) and ammonium wet deposition (bottom) for the US (top), EANET (middle) and EMEP (bottom) networks. The average values for 2010–2015 are shown. The dashed line denotes the 1:1 slope.

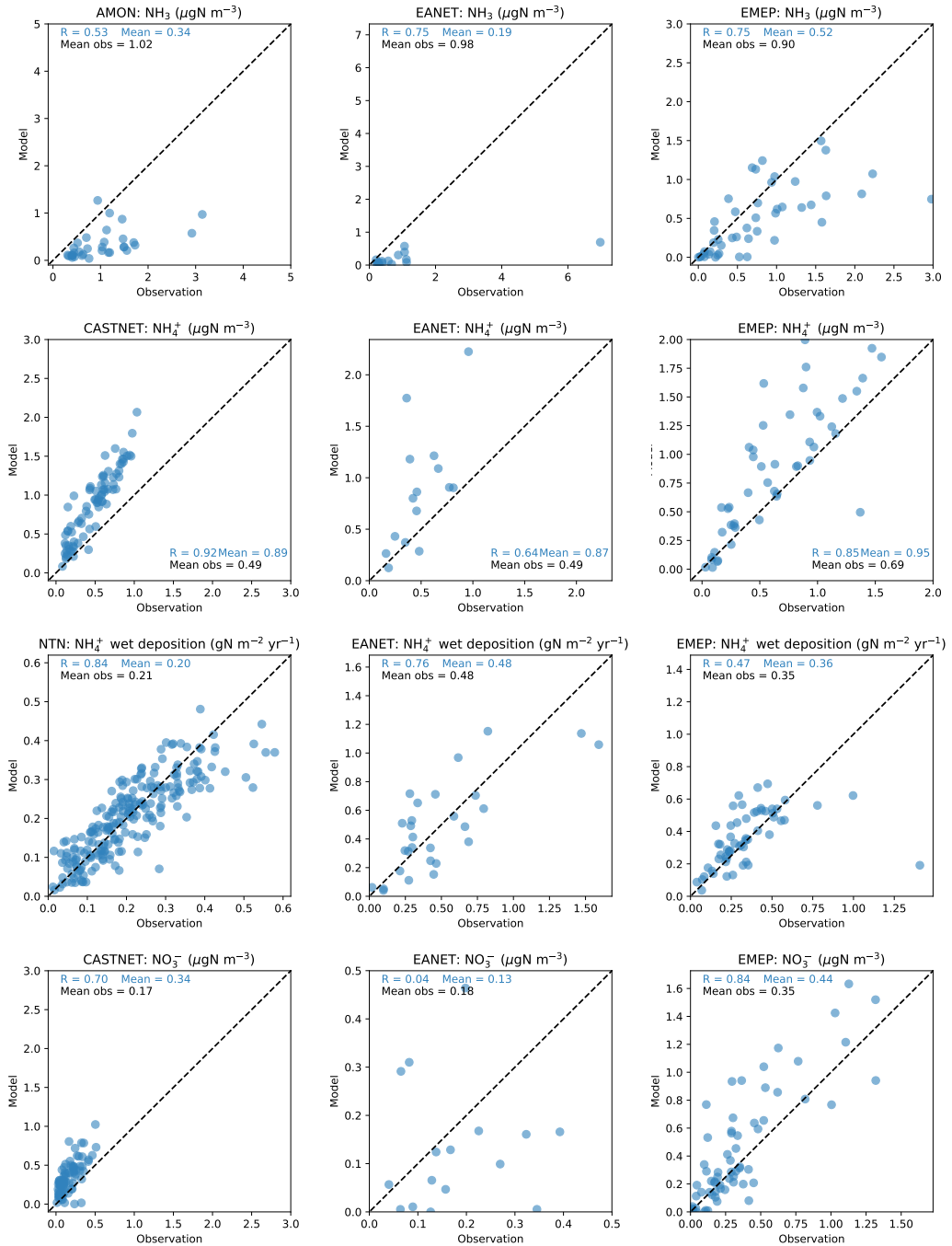


Figure S9: Same as Fig. S8 but for the CEDS run.

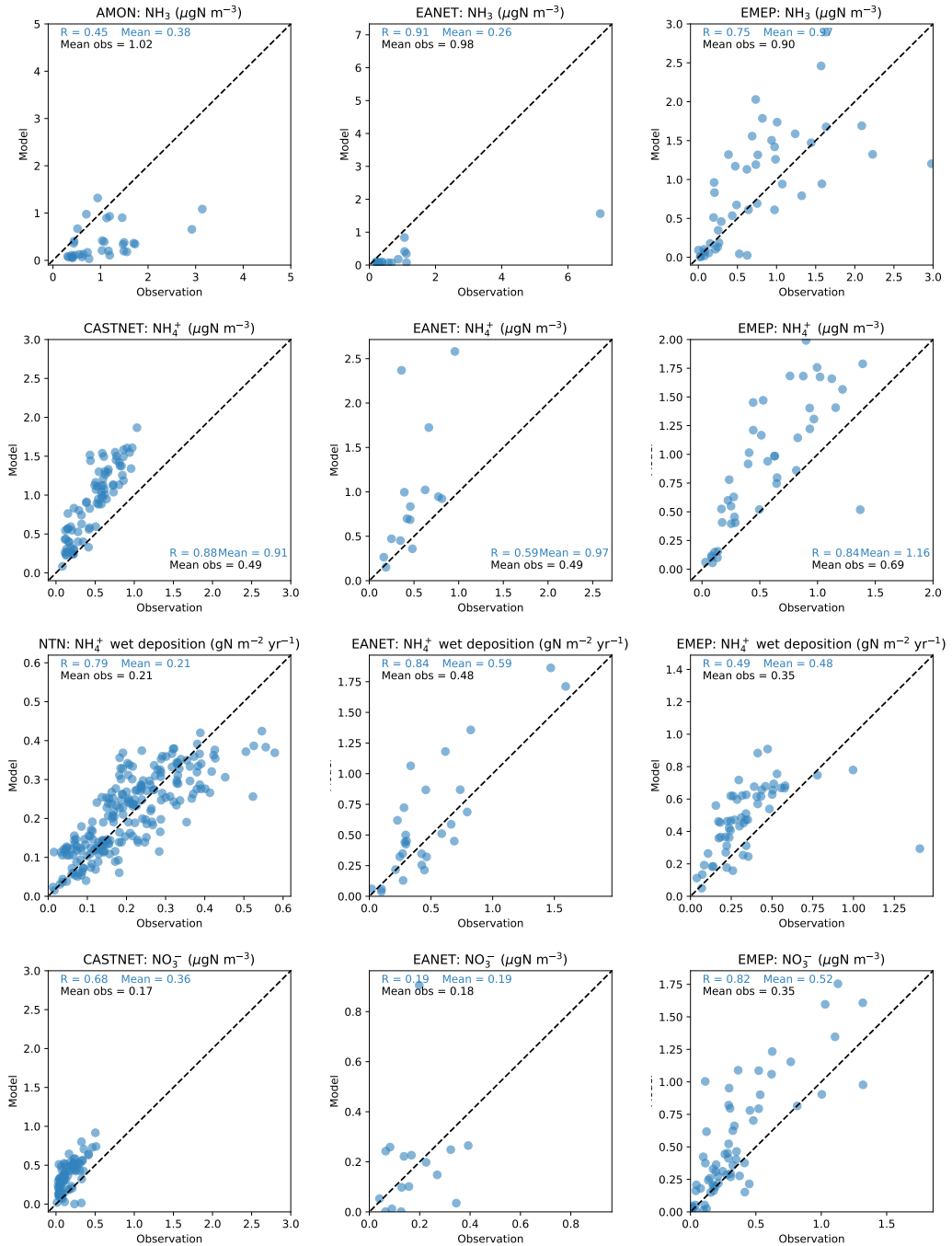


Figure S10: Same as Fig. S8 but for the EDGAR run.

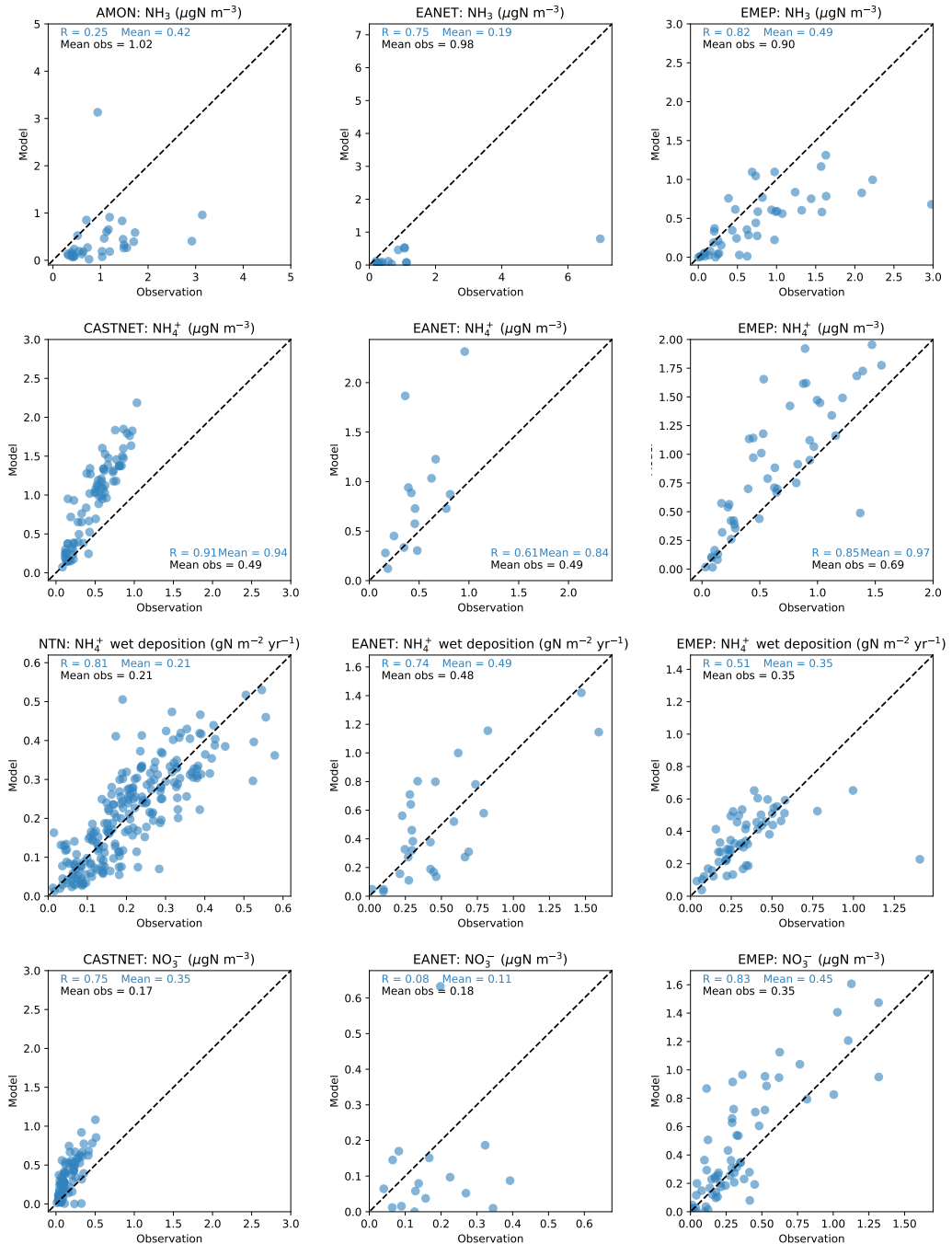


Figure S11: Same as Fig. S8 but for the HTAP run.

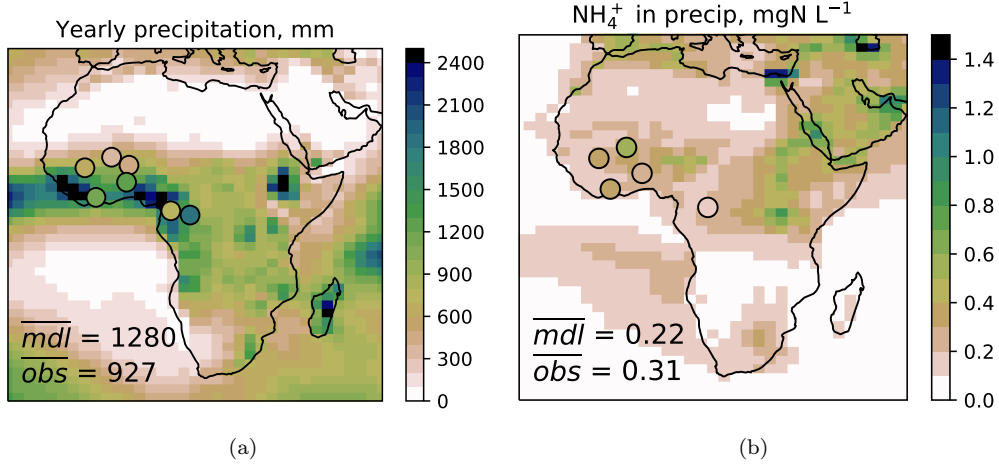


Figure S12: Modeled (a) yearly precipitation (mm) and (b) NH_4^+ concentration in precipitation (mgN L^{-1}) in the FAN simulation.

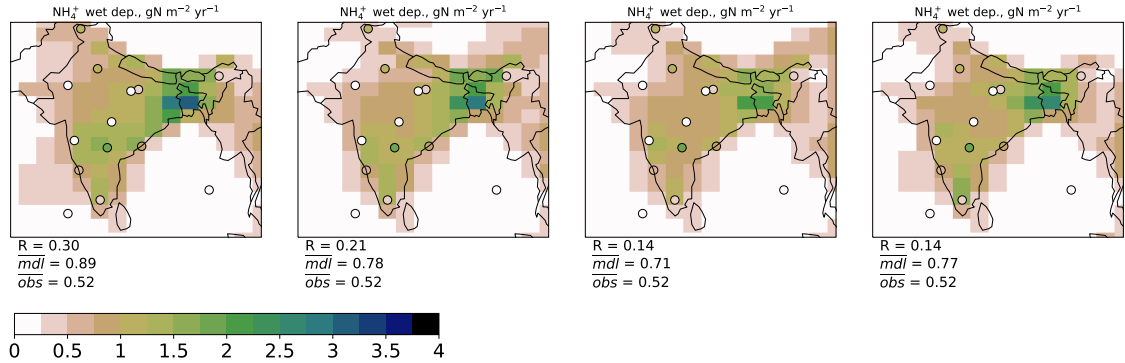


Figure S13: The modeled NH_4^+ wet deposition over India in the FAN, CEDS, EDGAR, and HTAP simulations ($\text{gN m}^{-2} \text{yr}^{-1}$; shading) and in the observations (Table A1; markers).

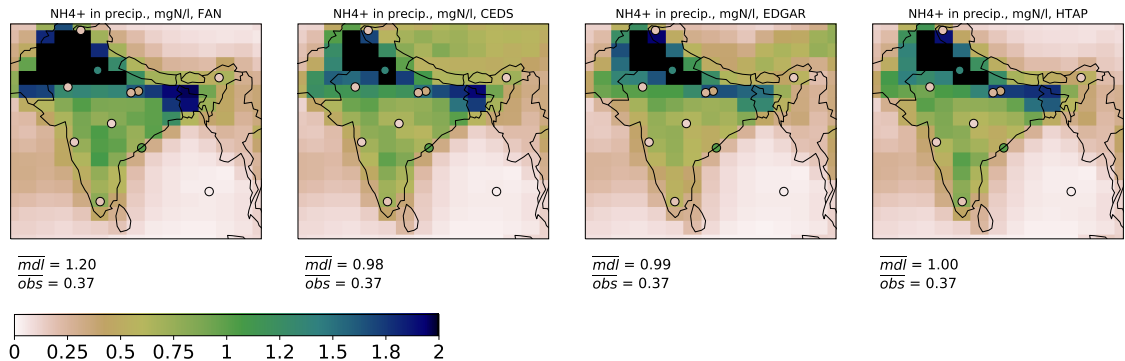


Figure S14: The modeled NH_4^+ concentration in precipitation over India in the FAN, CEDS, EDGAR, and HTAP simulations (mg N L^{-1} ; shading) and in the observations (Table A1; markers).

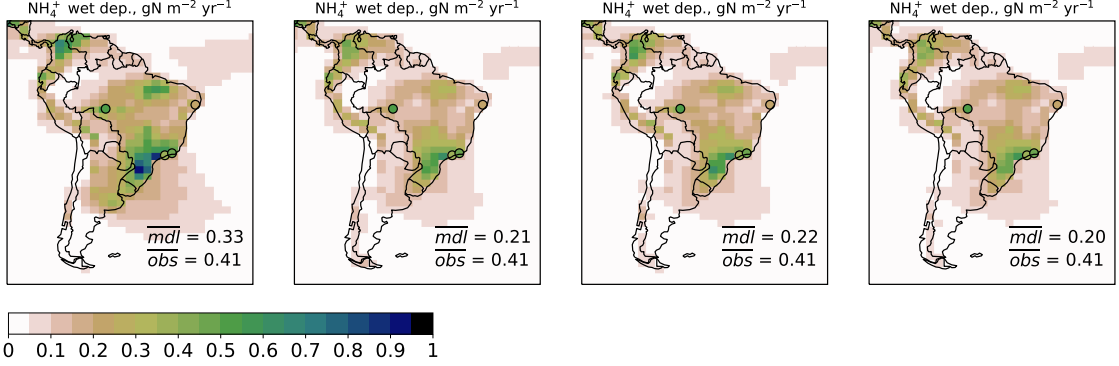


Figure S15: The modeled NH_4^+ wet deposition over South America in the FAN, CEDS, EDGAR, and HTAP simulations ($\text{gN m}^{-2} \text{yr}^{-1}$; shading) and in the observations (Table A1; markers).

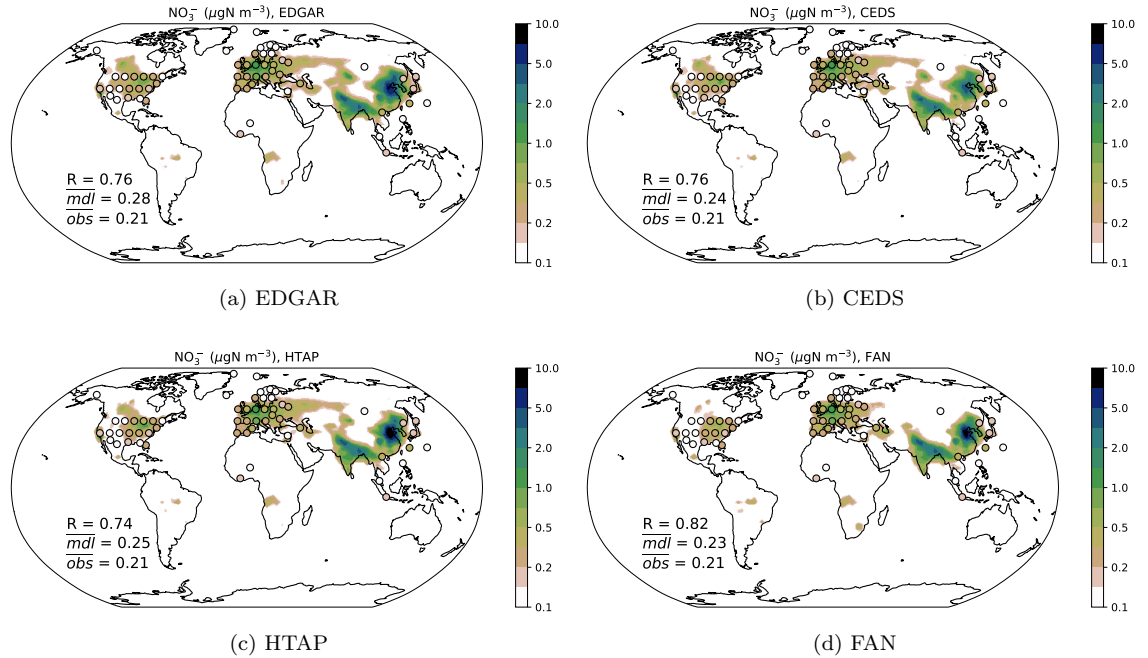


Figure S16: Average concentration of NO_3^- ($\mu\text{gN m}^{-3}$) in the EDGAR, CEDS, HTAP and FAN simulations for 2010–2015. Observed values are indicated by markers. The density of observations has been reduced as in Fig. 1

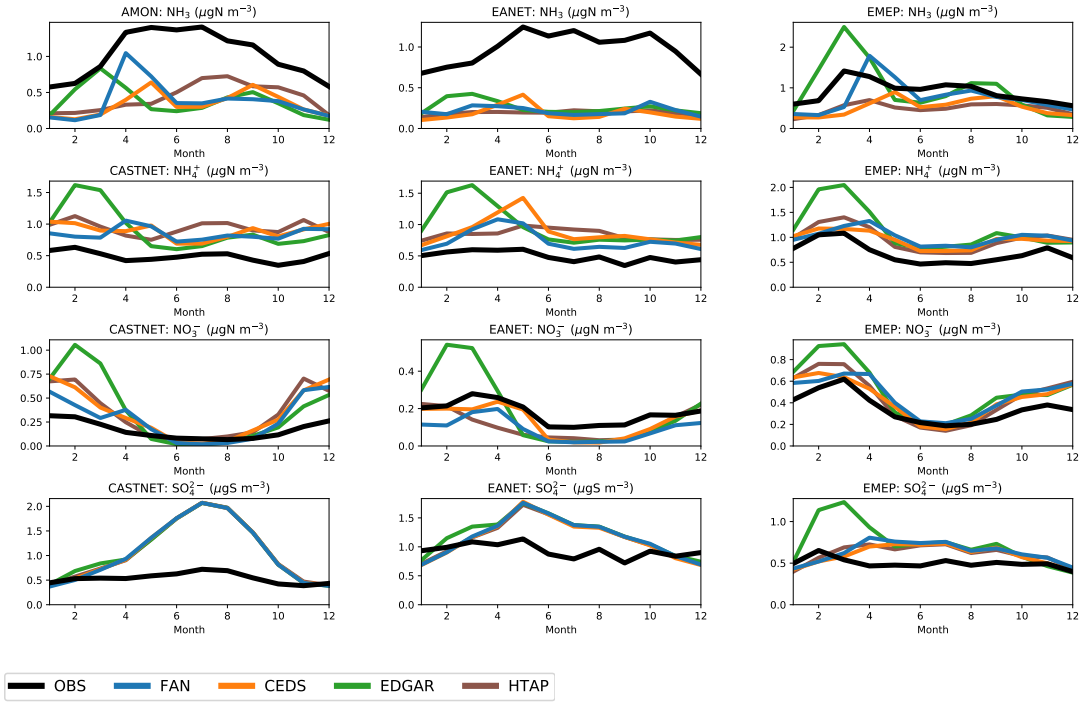


Figure S17: Seasonal profiles of simulated NH_3 , NH_4^+ , NO_3^- and SO_4^{2-} over the EANET, EMEP, and the North American (CASTNET and AMoN) networks. All values are averaged over the years 2010–2015.